A Combined Alignment and Registration scheme of Psoriasis Lesion Images

Gabriela Maletti and Bjarne Ersbøll

Department of Informatics and Mathematical Modelling,
Technical University of Denmark,
DK-2800 Kgs. Lyngby, Denmark
{gmm, be}@imm.du.dk
http://www.imm.dtu.dk/image

Abstract. A two-stage registration scheme of psoriasis lesion patterns is proposed. In the first stage, global rotation and translation effects of assumed equally scaled psoriasis lesion patterns are removed. In the second stage, only local translation effects are removed. In both stages a novel algorithm for extreme value detection is applied. The output of each stage is evaluated with the M.A.D. transform and the correlation coefficient. Results are shown for real examples.

1 Introduction

We use a set of segmented psoriasis lesion patterns from *RGB* images taken at the Gentofte Hospital, Denmark, during pilot sessions with three invited patients. For each patient, three lesions were followed once a week for at least three weeks. In each session, five images of each lesion were taken. Following the notation used in previous work ([13], [11], [12], [14]), the group of images corresponding to a given patient and lesion is here called "case (patient, lesion)". Part of the mentioned segmented patterns[1] was generated by a two-stage hierarchical classification scheme [11], and another part, was produced by user-interaction[2]. This was done so, in order to exclude shadow effects in the captured objects [12]. One case[3] was excluded, because corresponding points between sessions were hard to find, by visual assessment.

Once a spacial pattern has been segmented, morphological descriptors like area, perimeter, compactness, perimeter roughness, eccentricity, shape and texture can be estimated ([9], page 340). In order to register two spatial patterns, it is required that the descriptors are sensitive to the transformations (rotations, translations and/or changes of scale) whose effect we want remove trough a distance minimization process. This minimal distance between two objects is

[1] For the cases $(1, A)$, $(1, B)$ and $(1, C)$ see Figures 2 to 4 in [14]. For the cases $(3, B)$ and $(3, C)$, see Figures 7 and 8 respectively in [11]
[2] See Figure 5 in [11] for the case $(2, B)$. Case $(2, A)$ was generated in the same way.
[3] The case $(2, C)$ was hair all over.

assumed to be referred to the position, angle and scale for which the patterns are matching. When this distance is Euclidean and the minimization is done over rotations and scale of equally centered objects then we have the full Procrustes distance [3]; when the same is only done over rotations, then we have the partial Procrustes distance. Procrustes Analysis is a useful approach for aligning two landmark registered shapes [8]. For the case that these shapes are not landmark registered, the approach could be extended by setting some constraints, for instance, with regard to the topology given by the connectivity between the landmarks. A list of references to landmark-free approaches can be found in [3], page 305.

It could be nice to include textural information [6], [10], [1], [7], [20], [19] during the registration process. Previous work that combines shape with textural information was published in [18]. In the present work, it is assumed that the shape of the object is invariant to scale and that, for each pattern, the pixels locations are landmarks that have to be matched. It is assumed that the objects of largest size in the thematic map indicating lesions are corresponding. However, they could not have the same size. Therefore, the most convenient set of pixels that will define the set of landmarks to be registered has to be found through a distance minimization process.

The basic approach could be to compare the pixel values in their original form. However, there are many ways to transform the data and present them to a distance function. A review of linear and non linear decomposition approaches can be found in [8]. Since the red band of each single image is the most correlated with the first principal component of the image [13], it is from this band the pattern values are compared.

This work is composed of the following sections. First, a review of measures of distances and similarities is given. Secondly, a general algorithm to obtain the minimal distance between two patterns is proposed. In many cases, the cost of the estimation of the values of a function is expensive. Therefore, to obtain one of its extreme values (for instance, its minimum) could be carried out on a small representative data-set. Then, a section detailing a scheme that uses this algorithm to carry out the initial alignment of patterns follows. The initial alignment implies removing global translation and rotation effects of two assumed equally scaled patterns. The output of the initial alignment scheme is used by an internal local registration scheme described afterwards. In this case, it is assumed that the local rotation effects in the interior of the patterns are not significant, and only local translation effects in the interior of the patterns are removed.

2 Distances and Similarities

A mathematical representation of how close or similar two objects or data-sets or groups of observations are, is given by the distance. The selection of the measure of distance used changes the results. A short review of definitions follows from [15].

Definition 1. *Given two points $\boldsymbol{x}$ and $\boldsymbol{y}$, a real-valued function $d(\boldsymbol{x}, \boldsymbol{y})$ is a distance function if it has the following properties:*

- *symmetry:* $d(\boldsymbol{x}, \boldsymbol{y}) = d(\boldsymbol{y}, \boldsymbol{x})$;
- *non-negativity:* $d(\boldsymbol{x}, \boldsymbol{y}) \geq 0$;
- *identification mark:* $d(\boldsymbol{x}, \boldsymbol{x}) = 0$

Definition 2. *A metric is a distance for which also the following properties are satisfied:*

- *definiteness:* $d(\boldsymbol{x}, \boldsymbol{y}) = 0$ *if and only if* $\boldsymbol{x} = \boldsymbol{y}$;
- *triangle inequality:* $d(\boldsymbol{x}, \boldsymbol{y}) \leq d(\boldsymbol{x}, \boldsymbol{z}) + d(\boldsymbol{z}, \boldsymbol{y})$.

Definition 3. *A measure of similarity $s(\boldsymbol{x}, \boldsymbol{y})$ is such that it satisfies the following properties:*

- $s(\boldsymbol{x}, \boldsymbol{y}) = s(\boldsymbol{y}, \boldsymbol{x})$;
- $s(\boldsymbol{x}, \boldsymbol{y}) > 0$
- $s(\boldsymbol{x}, \boldsymbol{y})$ *increases as the similarity between* $\boldsymbol{x}$ *and* $\boldsymbol{y}$ *increases.*

Some frequently used measures of distances between two data-sets $\boldsymbol{x}$ and $\boldsymbol{y}$ are [21], [15]:

- Distance of Minkowsky

$$d(\boldsymbol{x}, \boldsymbol{y}) = (\sum_{i=1}^{m} |x_i - y_i|^r)^{\frac{1}{r}} \tag{1}$$

- Euclidean Distance

$$d(\boldsymbol{x}, \boldsymbol{y}) = \sqrt{\sum_{i=1}^{m} (x_i - y_i)^2} \tag{2}$$

- Distance of Manhattan

$$d(\boldsymbol{x}, \boldsymbol{y}) = \sum_{i=1}^{m} |x_i - y_i| \tag{3}$$

- Distance of Camberra

$$d(\boldsymbol{x}, \boldsymbol{y}) = \sqrt{\sum_{i=1}^{m} \frac{|x_i - y_i|}{|x_i + y_i|}} \tag{4}$$

– Distance of Chebychev

$$d(\boldsymbol{x}, \boldsymbol{y}) = max_{i=1}^{m}|x_i - y_i| \tag{5}$$

– Quadratic Distance

$$d(\boldsymbol{x}, \boldsymbol{y}) = (\boldsymbol{x} - \boldsymbol{y})^T Q(\boldsymbol{x} - \boldsymbol{y}) \tag{6}$$

where Q is a positive definite $m \times m$ matrix of weights.

– Distance of Mahalanobis

$$d(\boldsymbol{x}, \boldsymbol{y}) = (\boldsymbol{x} - \boldsymbol{y})^T V^{-1}(\boldsymbol{x} - \boldsymbol{y}) \tag{7}$$

where V is the covariance of $\boldsymbol{x}$ and $\boldsymbol{y}$.

– One minus Correlation

$$d(\boldsymbol{x}, \boldsymbol{y}) = 1 - |\frac{\sum_{i=1}^{m}(x_i - \overline{x})(y_i - \overline{y})}{\sqrt{\sum_{i=1}^{m}(x_i - \overline{x})^2 \sum_{i=1}^{m}(y_i - \overline{y})^2}}| \tag{8}$$

– Scalar Product [9]

$$d(\boldsymbol{x}, \boldsymbol{y}) =< \boldsymbol{x}, \boldsymbol{y} > \tag{9}$$

which can be standardized in different ways, like range, standard deviation or number of elements. Some more distance measures can be found in [17]. Similarity measures can be transformed into dissimilarity measures by means of tricks like [5]:

$$s(\boldsymbol{x}, \boldsymbol{y}) = \frac{1}{1 + d(\boldsymbol{x}, \boldsymbol{y})} \tag{10}$$

or

$$s(\boldsymbol{x}, \boldsymbol{y}) = c - d(\boldsymbol{x}, \boldsymbol{y}) \tag{11}$$

with c a constant.

In order to evaluate, for our registration problem, the appropriateness in using one of the measures of distances previously listed, the following aspects are considered:

– Feature space properties: results of clustering depend on the choice of the measure of distance.
– Set elements correspondence: the way the elements of two sets are ordered affects the measure of distance between the sets.
– Computational time: the number of mathematical operations required to obtain each given measure of distance is counted.

With respect to the feature space, Duda and Hart ([4], page 213) pointed out that the selection of the Euclidean distance (See Equation 2) implies that the feature space is isotropic: the clusters will be invariant to translations or rotations; however, they will not be invariant to linear transformations in general or to transformations that distort the distance relationship. In order to achieve invariance the data can be normalized prior to clustering. Normalization implies the introduction of information that gives the procedure meaning. Some normalization suggestions given in [4] are, for instance:

- invariance to displacements and scale changes: translate and scale the axes so that all the features have zero mean and unit variance. This prevents certain features from dominating distance calculations. This approach is appropriate if the spread of the values is due to normal random variation. The problem with our data set is that, for instance, changes in the class variances could be of interest to detect lesion changes in time. For instance, when scaling appears in the lesion, the variance of the distribution changes. This means, that a normalization by variance of the original data is not the most appropriate decision. Furthermore, changes in the redness of the lesions, which imply mean class displacements along the time, are also of interest for the dermatologists.
- invariance to rotation: rotate the axes so that they coincide with the sample covariance matrix (transformation to principal components). This can be preceded or followed by normalization for scale.

Many other normalized distance or similarity functions could be used to normalize the data.

With respect to the pixel correspondence, the following is considered. When data sets are compared, the order given to the elements of each single set (i.e. the correspondence established between pairs of same indexed elements, one of each set) plays a relevant role. Note, for instance, in the equations of distances given, that the index i establishes the correspondence between the $i-th$ element of the set $\boldsymbol{x}$ and the $i-th$ element of the set $\boldsymbol{y}$. For our case, by placing a rotated and translated version of a pattern over another pattern, and computing a measure of distance, location correspondence of pixels could be assumed. On the other hand, as it was mentioned before, spatial registration of patterns requires descriptors sensitive to the transformations that are expected to be removed. However, for prediction purposes, it could be nice to use descriptors invariant to the transformations that need to be removed in order to achieve registration of patterns, like the normalized histogram or the co-occurrence matrix (See [14]).

Results obtained regarding to the computational time can be seen in Table 1. As it can be deduced, Equation 3 has the smallest computational cost.

3 The Extreme Value Detection Algorithm

The Extreme Value Detection Algorithm (E.V.D.A.) is an iterative process that assumes that the expected minimum (extreme value) of the distance function between two objects is near the center of masses of the domains of those objects. In the first iteration, a mapping template centered on the center of mass of the domain of one of the objects is used to define the subset of the domain of the distance function for which their values will be estimated. This mapping template includes many points of the neighborhood of the center of mass, and only

Table 1. Number of operations required for the computation of each measure of distance between two $d-$dimensional vectors $\boldsymbol{x}$ and $\boldsymbol{y}$ of m elements, with $d = 1$.

Distance	+	−	∗	/	||	^	if	Order
Minkowsky	m	m		1	m	m+1		4m+2
Euclidean	m	m				m+1		3m+1
Manhattan	m	m			m			3m
Camberra	2m	m		m	2m			6m
Chebychev		m			m		2m	4m
Quadratic	2m	m	2m					5m
Mahalanobis	3m	2m	2+m	3				6m+5
Correlation	5m	4m	m+1	1		2m+2		12m+4

few that are far away of the center. The extreme value of the calculated values of the distance function is obtained, and the same mapping template is centered on that first guess of the extreme value. This step is repeated until the guessed extreme value does not change anymore.

Formally, the Extreme Value Detection Algorithm (E.V.D.A.) is an algorithm that iteratively approximates the extreme value f_{ext} (minimum or maximum) of a smooth and discrete function F defined over a subset L_F of a lattice $L = \{[r, c] | 1 \leq r \leq M, 1 \leq c \leq N\}$, such that the location of f_{ext} is $[r, c]_{ext}$ and f_{ext} is unique. For each iteration, a mapping template is centered on the position of the actual guess $\hat{[r, c]}_{ext}$ of the location of that extreme value. This template is Bolduc and Levine's [2] three parameters retinal mapping model $M(r_f, \omega, \alpha)$, where:

- r_f is the foveal radius,
- ω is the receptive field overlap factor, and
- α is the receptive field size-to-eccentricity ratio, (the size of the receptive field is the diameter of the receptive field circle, and the eccentricity of a receptive field is, in our case, the radial distance from the center of the receptive field to the actual guess $\hat{[r, c]}_{ext}$ of the location the extreme value).

The initial actual guess of the location of the extreme value can be any element of L_F (the use of the center of mass of the domain is suggested). Following Bolduc and Levine's model, receptive field centers are arranged along rays originated at $\hat{[r, c]}_{ext}$, and along circles also placed at the same location (See Eq. 1-3 of [2] for details of the derivation of the positioning parameters θ and k, where θ is the angle between adjacent rays and k is the ratio of radii of adjacent circles). The circle of radius r_{nr} is such that it is the circle of maximum radius for which at least one point belongs to L_F. The function F is computed for each center of receptive fields placed on the rings and for each element belonging to the fovea. The location of f_{ext} guessed for the next iteration is given by the location of the extreme value $\hat{f}_{ext}$ of F computed until now. If more than one element of L_F can be the actual guess, then one of them is randomly selected. The algorithm stops when the values of $\hat{[r, c]}_{ext}$ between two consecutive iterations do not change

anymore. The convergence is guaranteed.

E.V.D.A. has a maximal processing time of $O(n_{r_f} + nr * (round(\frac{2*\pi}{\theta})))$ per iteration, where n_{r_f} is the number of elements of the fovea, nr is the number of rings and $round((\frac{2*\pi}{\theta}))$ is the number of receptive fields placed on each ring. It has a fast convergence because, for each iteration, a local neighborhood of the estimated minimum value composed of the elements of the fovea is analyzed in detail, at the same time other parts of the whole domain are taken into account by sampling the centers of receptive fields placed over rings of increasing radius at a logarithmic scale.

Some examples of mapping templates are shown in Figure 3.

The E.V.D.A. has been tested using Wilson's Model [22] parameters ($\omega = 0.5$ and $\alpha = 0.25$) on lattices of 100 by 100 elements. The foveal radius was increased from 1 to 50. For each foveal radius, the algorithm was tested 20 times. The initial guess of the location of the extreme value was randomly set. The minimum values of the following functions were found:

Table 2. Tested functions

Nr.	Function	Domain
1	$Z = (X^2 + Y^2)^{-\frac{1}{2}}$	$L_Z = \{[r, c] \mid -99 \leq r \leq 0, -99 \leq c \leq 0\}$
2	$Z = (X^2 + Y^2)$	$L_Z = \{[r, c] \mid -49 \leq r \leq 50, -49 \leq c \leq 50\}$
3	$Z = 1 - \frac{1}{(X^2+Y^2+1)}$	$L_Z = \{[r, c] \mid -49 \leq r \leq 50, -49 \leq c \leq 50\}$
4	$Z = 1 - \frac{1}{(X^2+Y^2+1)}$	$L_Z = \{[r, c] \mid -89 \leq r \leq 10, -69 \leq c \leq 30\}$

For each function and foveal radius, the number of estimated function values and the average number of iterations is shown in Fig. 2. Note that for all the testing functions, being the convergence guaranteed, the percentage of evaluated points increases unnecessarily when the foveal radius increases. The cases for which the function is not smooth, contextual information could be useful.

4 Initial alignment

Some definitions to be used in the present section are first introduced. Afterwards, an algorithm to carry out the initial alignment is proposed.

Given a set of segmented patterns of a given lesion, in the initial alignment stage, global translations and rotations effects between pairs of patterns are removed. For comparison purposes, it is assumed that the dispersion of the elements of the data-sets is of interest, while the mean differences are not. Some

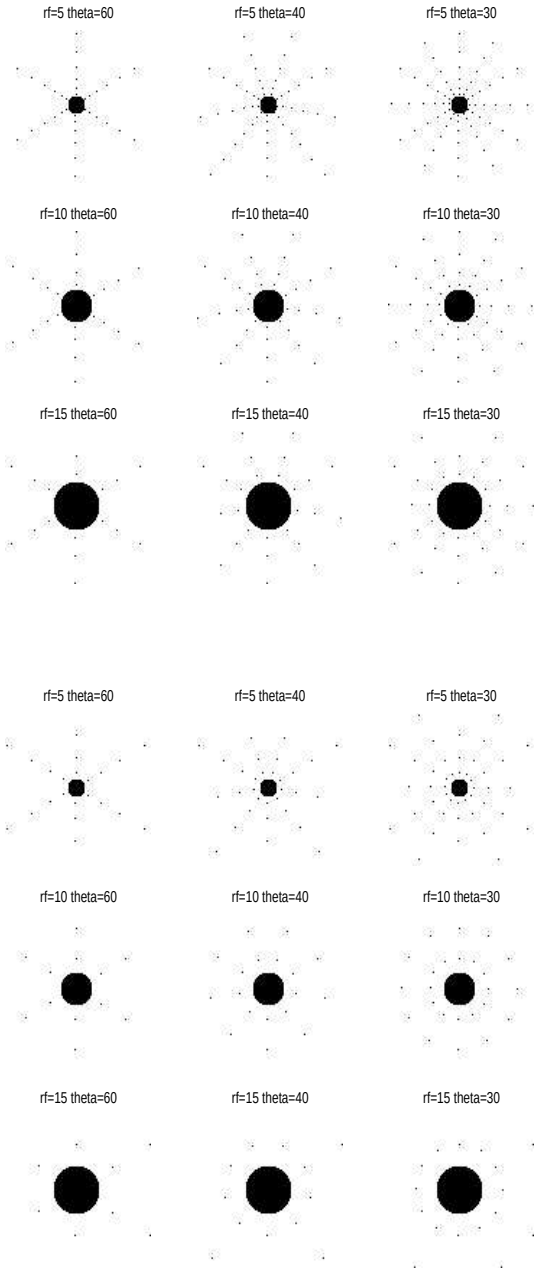

Fig. 1. Mapping templates
They are shown on a domain of 100 by 100 pixels of size with different foveal radius ($r_f = 5, 10, 15$ pixels) and different angles between adjacent rays of ($\theta = 60, 40, 30$ degrees) for the positioning parameter $k = 0.4$ (first three rows) and $k = 1$ (last three rows).

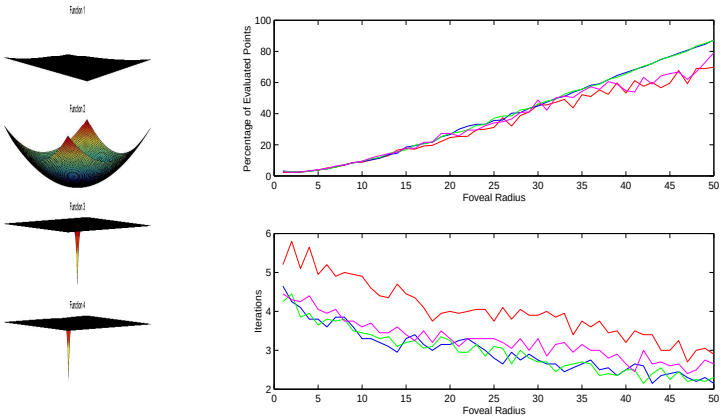

Fig. 2. Tested functions and results of the Extreme Value Detection Algorithm for foveal radius varying from 1 to 50.

definitions follow:

Definition 4. *Let two windows A and B of size $n_a = n_b$ with domains L_A and L_B such that $\exists \boldsymbol{t} \wedge \hat{\theta}$ for which:*

$$L_B = Rot[Trans[L_A, \boldsymbol{t}], \hat{\theta}] \tag{12}$$

where Rot and $Trans$ are the rotation and translation function respectively defined in a 2-D discrete space. Rot and $Trans$ are commutative.

For each window, we compute a texture descriptor, and then take a measure of distance between pairs of windows. The measure of distance used is Manhattan distance (See Equation 3). The texture descriptor is the volume under the surface formed by the normalized values of the pixels of the window. In this way, the quantization level information is removed, while the texture is preserved.

Definition 5. *The difference of volume $dV_{(A),(B)}$ between the windows A and B is, in general, defined as:*

$$dV_{(A),(B)} = dV_{(B),(A)} = \frac{1}{2} \sum_{i=1}^{n_{A \cap B}} |w_{(A)}[i] - w_{(B)}[i]| \tag{13}$$

where, in the present work,

$$w_{(J)}[i] = \frac{x_{(J)}[i]}{\sum_{i=1}^{n_J} x_{(J)}[i]} \tag{14}$$

$x_{(J)}[i]$ is the value of the pixel located at the $i-th$ position of the $J-th$ window of n_J elements. Note that $0 \leq dV \leq 1$.

During the initial alignment, it is assumed, for a given lesion, that Equation 12 is true for the intersection of the translated and rotated versions of the pair of pattern domains, for which the distance (see Equation 13) between the corresponding pixel values is minimal. It is also assumed that the objects to be aligned have the same scale. However, as mentioned before, the input of the initial alignment stage is a set of segmented patterns (this means, the overlaps between segmented objects indicating lesion and the original data), which may not have the same area. (See, for instance, Figures 2 to 4 in [14]). The most important result produced by this stage is the specification of the number of landmarks to be registered in a next stage, this means, that the area of the objects is finally forced to be constant. Since some lesion patterns are occluded in the original images, it is left to the user to decide if the number of landmarks is given by the area of the intersection of the whole set or of a subset of the aligned domains (objects in thematic maps indicating lesion).

The algorithm that carries out the initial pattern alignment is detailed here. First, the n largest sized objects belonging to each of the thematic maps obtained in the previous stage are found. Misclassified pixels forming holes within regions indicating lesions are previously assigned to the class lesion[4]. Correspondence by decreasing object area is assumed. From now, it is assumed that the overlay of the object with the pixel values is a window. For each given window S and a given reference window R, each of the rotations $Rot(R, \hat{\theta})$ is centered on the position of each pixel of S, and the angle $\hat{\theta}_{opt}$ and location $[i, j] \in L$ for which the difference of volume is minimal is found. L is the lattice on which the images including the patterns R and S are defined. In practice, pattern objects are rotated in a range varying from -45 to 45 degrees. For each iteration, this range is divided into five intervals. Neighboring intervals containing the minimum of the evaluating function dV (Equation 13) define the range for the next iteration. This minimum is computed using the Extreme Value Detection Algorithm (E.V.D.A.) detailed in Section 3. The algorithm stops when the minimum between two iterations differ with less than a user-provided threshold β.

The output of the initial alignment stage is back-projected to the original data and a new set of images containing the aligned shapes is obtained. These images can afterwards be registered and realigned.

[4] The function *bwfill* of Matlab Version 6.1.0.450 (R12.1) is used.

4.1 Results and Discussion

The following parameters were set for the initial alignment of the lesions:

- The threshold β for the minimal angle was 1 degree.
- One object per thematic map was tracked within and between sessions related to the same lesion.
- For all the cases, the mapping template used was $M(0.3, 0.5, 0.25)$. The first parameter in M is a percentage of the smallest side of the smallest rectangle that includes the lesion. The last parameters correspond to Wilsons's Model.
- The lesion pattern of the first image of each sequence was the reference window S.
- The initial alignment with original red band data is presented here.

The Algorithm E.V.D.A. defines searching areas starting from the center of mass of the pattern domain, because it is expected that the maximum overlap between a pair of pattern domains will be near their center of masses.

The number of computations of values of the minimizing function F decreases along the iterations, because values of previous iterations can be preserved.

The set of aligned lesion patterns can be seen in Section A. For all the cases, 10 rows and columns were removed from the borders. For the cases $(1, A)$, $(1, B)$, $(1, C)$, $(3, B)$ and $(3, C)$ the classification outputs were used; this means that the image data were down-sampled with a factor of 4 [5]. For the cases $(2, A)$ and $(2, B)$ no down-sampling was done.

The Extreme Value Detection Algorithm used on average 3 iterations. Clearly, the use of a template providing the same amount of information for each ring, while the spacing between rings is given at a logarithmic scale, is advantageous for the fast detection of the emergence of an extreme value in the sampled domain. On the other hand, looking for the extreme value in the same location as the center of the domain of the reference window is a reasonable criteria, that helps to reduce the convergence time. This is added to the fact that the sampling rate is increased in the foveal region. However, it has to be mentioned that some extended tests have shown that if the initial guess of the position of the extreme value was too far away from the real value, the algorithm stopped in a local extreme value.

In general, it can be said that, by visual examination, the results are satisfactory. Looking through some of the alignment results, it is obvious that the illumination problem is greater than expected. See, for instance, how much the shadow location varies in the case $(3, A)$. In fact, as it was reported in [12], the shadows do affect the classification results. However, a comparison of the alignment results before and after illumination correction, which is shown in

[5] One pixel every four columns and rows was selected.

Appendix B, is given only as an illustrative example [6]. Correlation values before and after illumination correction are compared in Table 3. Details can be found in Table 9.

Table 3. Average correlation and standard deviation of a randomly selected aligned lesion pattern of the lesion A of the patient 2 with the remaining aligned lesion patterns of the same patient and lesion.

(2,A)	μ_R	σ_R	μ_G	σ_G	μ_B	σ_B
Before	0.5650	0.1195	0.3819	0.1103	0.4824	0.0755
After	0.3173	0.0568	0.2292	0.0489	0.1919	0.0470

Even when the illumination was corrected, the initial alignment results did not improve. May be the measure of distance used gets a bit confused in large data-sets. Note in the fourth and fifth capture of the first session of the case $(3, B)$, that the E.V.D.A. clearly stopped in a local minima, and it was not able to align the data correctly. This could imply that the measure of distance is less sensitive to changes when the data set is too large. This alignment problem is, in fact, not trivial. The intersection of the pattern domains was used to define the region for which the measure of distance is computed. When the pattern domains are (almost) overlapping, the area of this region is maximal. We expect a minimal difference of volume near the center of masses of the domains. For this reason, the initial alignment of the pattern corresponding to the first patient, for which the pattern domains were very similar, worked very well. However, for the most of the remaining cases, the patterns do not have a common shape: some lesion borders are given by the image border. We could think of different scale-shapes, or what is more precise, after an ideal alignment, the intersection of the domains is far from being equal to the union of the domains. Therefore, the E.V.D.A. finds a minimum when the overlap of the patterns domains is near a maximal and not where the patterns have a maximal overlap. To find the minimal intersection sample size prior to the alignment could probably improve the results.

On the other hand, it is mentioned only as a comment, that the initial alignment output using the $|B - G|$ lesion data was satisfactory for the cases $(1, A)$, $(1, B)$, $(1, C)$ and $(3, C)$. However, particularly for the cases $(3, A)$ and $(3, B)$ it was not possible to align the whole data set in an acceptable way. May be due to the same reasons as explained before.

[6] Due the high contrast between the lesion and the rest, in both cases, the $|B - G|$ band. The images where down-sampled a factor of 16: one pixel every 16 columns and rows was selected.

For a given lesion, the expected correlation value of a randomly selected aligned lesion pattern with any other remaining aligned pattern of the same set (case) is given in Table 4. The values of each single μ cell were computed according to the following equation:

$$\mu_{p,l,b} = \frac{1}{n_s n_c} \sum_{i=1}^{n_s} \sum_{j=1}^{n_c} E[corr(\mathsf{X}_{p,l,i,j,b}, \mathsf{X}_{p,l,:,:,b})] \tag{15}$$

where $E[corr(\mathsf{X}_{p,l,i,j,b}, \mathsf{X}_{p,l,:,:,b})]$ is defined as:

$$E[corr(X_{p,l,s,c,b}, X_{p,l,:,:,b})] = \frac{1}{n_s n_c - 1}(\sum_{i=1}^{n_s} \sum_{j=1}^{n_c} corr(X_{p,l,s,c,b}, X_{p,l,i,j,b}) - 1) \tag{16}$$

and p is the index for patient, l, for lesion, s, for session, i, for capture, b for color band. The symbol n_c is the number of captures of the $s-th$ session. The session s takes values in {'a','b','c','d'}, where the order in the sequence indicates the session week. The symbol n_s is the number of sessions. The color band b takes values in {'R','G','B'}.

The values of each single σ cell were computed according to the following Equation:

$$\sigma_{p,l,b} = \sqrt{\frac{1}{n_s n_c} \sum_{i=1}^{n_s} \sum_{j=1}^{n_c} (E[corr(\mathsf{X}_{p,l,i,j,b}, \mathsf{X}_{p,l,:,:,b})] - \mu_{p,l,b})^2}. \tag{17}$$

where the sub-indices have the same meaning as before.

Table 4. Average correlation and standard deviation of a randomly selected aligned lesion pattern with the remaining aligned lesion patterns of the same patient and lesion, per color band, patient and lesion.

(Patient, Lesion	μ_R	σ_R	μ_G	σ_G	μ_B	σ_B	$\mu_{\|B-G\|}$	$\sigma_{\|B-G\|}$
(1,A)	0.6918	0.0468	0.5770	0.0538	0.3679	0.0595	0.6941	0.0323
(1,B)	0.6696	0.0932	0.5241	0.0944	0.4413	0.0843	0.4517	0.1305
(1,C)	0.2534	0.0806	0.1651	0.0642	0.1138	0.0561	0.4211	0.0585
(2,A)	0.5162	0.0606	0.3561	0.0589	0.5720	0.0588	0.6486	0.0367
(2,B)	0.6681	0.0227	0.5736	0.0331	0.7260	0.0219	0.4854	0.0432
(3,C)	0.2550	0.0288	0.0757	0.0350	0.1289	0.0202	0.3524	0.0672

5 Combined registration and alignment

According to the experience of the dermatologist that lesions with psoriasis do not significantly change their shape and size along the time: the major change

happens within the lesions instead. After the initial alignment it is assumed that the aligned patterns have the same size and shape. Until now, for a given lesion, elements of pairs of aligned patterns located at the same position were considered corresponding points. This hypothesis is now refined: we assume that there is some error produced by small internal displacements. These displacements are assumed to be small translations only.

In the first part of the present Section, a novel registration scheme is proposed. This scheme uses the E.V.D.A. (See Section 3) and thin plate spline interpolations, the theory of which was included for completeness. A subsection of results and discussion follows.

5.1 A registration scheme

In general, in order to define the correspondence, two m-dimensional sets of landmarks T and Y, called the source and the target respectively have to be specified [3]. In the present scheme, $m = 1$ and, for each given image taken during a given session, the source T is given by the locations of pixels belonging to the aligned pattern corresponding to the first image of the first session, and the target Y should be given by their corresponding but unknown locations of pixels. In order to reduce the computational time, for each pattern, only a subset of T and Y is considered at first. Pixels placed on a grid composed of square cells with a user-defined number of points form the subset of T for which their corresponding points will be found. The correspondence between the source subset and the target subset is established as follows. For each pixel belonging to the grid, a user-defined circular neighborhood is considered. At the same location in the second image, another user-defined circular neighborhood[7] - larger than the previous one[8]- is taken into account. See an example in Figure 3. The difference of volume values dV of all[9] the translations of the first window over the second window are considered. The position of the pixels belonging to the second image whose neighborhood has the minimal difference of volume compared to the window of reference the pattern is saved in a new grid.

Afterwards, two different approaches are considered:

– Approach 1: The window sizes defining the searching areas in the target image are reduced along the iterations. The process is repeated, but a target pixel is moved to a new position only if the difference of volume between the source window and the new guess of the estimated corresponding target window is smaller than the difference of volume between the source window

[7] These window sizes are established by visual inspection of the image containing the error between pairs of images taken during the same session.
[8] Computed as a function of the spacing between the points on the grid
[9] In practice, only the points defined by the mapping template used in E.C.V.A. were evaluated

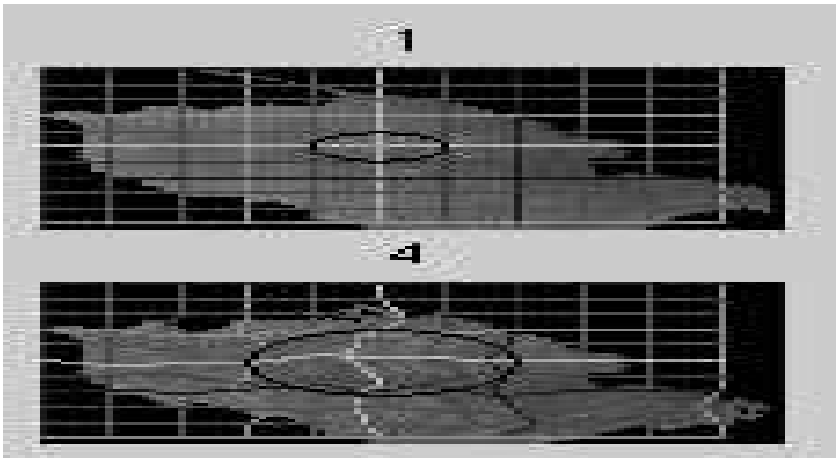

Fig. 3. Pair of corresponding grids for two segmented lesions of the case $(1, B)$ .On the right, the user-defined grid with one example neighborhood delineated in black. On the left, the corresponding grid with the evaluating neighborhood of the example on the right.

and the actual guess of the estimated corresponding window. The user is repeated for a user-provided number of iterations.

- Approach 2: The average grid is computed. The set of distance vectors from the grid of the reference pattern image to the average grid is used to translate all the grids to a new position. This process is repeated for a user-provided number of iterations.

Then, to generate the whole target set Y for each single image, thin plate splines are applied to the rest of the values of the source T and the rest of the new lesion image can be generated (See Section 5.2).

At the end of this stage, it is expected that the pattern correlation within and between sessions increases. Also, when comparing two patterns belonging to the same session, randomly Gaussian noise should be observed in their difference.

5.2 Pairs of thin-plate splines

This topic is described following Dryden and Mardia [3]. Conceptually, the thin-plate spline is the most natural interpolating function for data in two dimensions, because it minimizes the amount of bending in transforming between two configurations.

Let the set of 2-dimensional landmarks be $\mathsf{T} = [\boldsymbol{t}_1\boldsymbol{t}_2...\boldsymbol{t}_k]^T$, on the first figure mapped exactly into $\mathsf{Y} = [\boldsymbol{y}_1\boldsymbol{y}_2...\boldsymbol{y}_k]$ on the second figure, with $m = 2$. There

are $2k$ interpolation constraints:

$$(\boldsymbol{y}_j)_r = \phi_r(\boldsymbol{t}_j), r = 1, 2, j = 1, ..., k \tag{18}$$

and $\phi = (\phi_1(\boldsymbol{t}_j), \phi_2(\boldsymbol{t}_j))^T$ for the 2-dimensional deformation.

A set of k pairs of thin-plate splines is given by k bivariate functions

$$\phi[T] = (\phi_1[T], \phi_2[T])^T \tag{19}$$

where

$$Y_{kx2} = [S^T_{kxk}\mathbf{1}_{kx1}\, T_{kx2}][W^T_{2xk}\boldsymbol{c}_{2x1}A_{2x2}]^T \tag{20}$$

where $S_{i,j} = \sigma(t_i - t_j)$ and $\sigma(h) = ||h||^2 log(||h||)$ if $||h|| > 0$ and 0 in the contrary case. Obviously, $S = S^T$. In order to define the bending energy, six more constraints are introduced:

$$[\mathbf{1}^T_{1xk}0_{1x1}\mathbf{0}_{1x2}][W^T_{2xk}\boldsymbol{c}_{2x1}A_{2x2}]^T = \mathbf{0}_{1x2} \tag{21}$$

$$[T^T_{2xk}\mathbf{0}_{2x1}0_{2x2}][W^T_{2xk}\boldsymbol{c}_{2x1}A_{2x2}]^T = 0_{2x2}. \tag{22}$$

Pairs of thin-plate splines which satisfy the constraints of Equation 21 and 22 are called natural thin-plate splines. Let the matrix symmetric positive definite matrix $\Gamma_{(k+3)x(k+3)}$ be defined with the left side matrix of Equations 20, 21 and 22 as follows:

$$\Gamma = \begin{pmatrix} S^T & 1 & T \\ 1 & 0 & 0 \\ T^T & 0 & 0 \end{pmatrix} \tag{23}$$

The inverse of γ exists if S^{-1} exists. Writing the partition of γ^{-1} as:

$$\begin{pmatrix} \Gamma^{11}_{kxk} & \Gamma^{12} \\ \Gamma^{21} & \Gamma^{22} \end{pmatrix} \tag{24}$$

we have that $W_{kx2} = \Gamma^{11}_{kxk}Y_{kx2}$ and $\Gamma^{21}_{1xk}Y_{kx2} = [c^T_{1x2}A^T_{2x2}]$

5.3 Results and Discussion

The following parameters were set to produce the outputs:

- The number of points in the grid was set to a multiple of 10. The minimum side of the smallest rectangle that includes the lesion was divided in ten pieces; the size of each piece defined the size of square cells forming the grid.
- The radii of the circular window sizes used for the registration were a function of the separation between points in the grid. For the source image, the radius was 1 times the separation between points in the grid; for the target image, it was 2.

- The mapping template was $M(0.30, 0.5, 0.25)$.
- The user-defined number of iterations was 10.
- The red band values were used for both approaches.
- For each case, the lesion pattern of the first image of the first session was used as the reference window.

Initially, occluded lesions were handled in the same way as the others. However, this considerably affected the results. After removing them from the sets to be registered, the algorithm was again applied and the results were more satisfactory.

Clearly, the separation between points in the grid is crucial during the registration stage, because the size of the source and target window depends on it: if the window size for the target image is too small, the error in the registration is not randomly distributed within the lesion and some structure appears. Too large window sizes, in some cases, only increased the computational time. Thus, they have to be selected after visual inspection of the difference between pairs of initially aligned lesions belonging to the same session. Setting these parameters per lesion could improve the results.

The registration outputs of the second approach are presented in Section C. Each single cell value in these tables was computed using Equation 16. In correspondence with Table 4, but using the correlation values of registration outputs, Tables 5 and 6 were generated.

Table 5. Average correlation and standard deviation per color band, patient and lesion of a randomly selected registered (with Approach 1) lesion pattern with the remaining patterns of the same patient and lesion.

(Patient, Lesion	μ_R	σ_R	μ_G	σ_G	μ_B	σ_B	$\mu_{\lvert B-G\rvert}$	$\sigma_{\lvert B-G\rvert}$
(1,A)	0.6917	0.0458	0.5670	0.0438	0.3682	0.0557	0.6582	0.0319
(1,B)	0.6772	0.0724	0.5364	0.0769	0.4605	0.0697	0.4086	0.1129
(1,C)	0.2768	0.0723	0.1902	0.0582	0.1313	0.0452	0.4150	0.0586
(2,A)	0.5451	0.0635	0.3686	0.0629	0.5779	0.0619	0.6031	0.0535
(2,B)	0.6624	0.0235	0.5737	0.0328	0.7097	0.0195	0.4107	0.0367
(3,C)	0.2811	0.0396	0.0821	0.0292	0.1410	0.0225	0.3246	0.0515

Averages per color band of the values of the Tables included in Section C are shown in Tables 7 and 8. In Table 7, each single cell value is the average per color band of only the correlation values within sessions (i.e. rows (a, a), (b, b), (c, c) and (d, d)). In Table 8, each single cell value is the average per color band of all the correlation values within and between sessions (this means, from rows (a, a), (a, b) ... to (c, d), (d, d)). Note that the second registration approach has a better performance than the first registration approach. However, the improvement in

Table 6. Average correlation and standard deviation per color band, patient and lesion of a randomly selected registered (with Approach 2) lesion pattern with the remaining patterns of the same patient and lesion.

(Patient, Lesion	μ_R	σ_R	μ_G	σ_G	μ_B	σ_B	$\mu_{\lvert B-G\rvert}$	$\sigma_{\lvert B-G\rvert}$
(1,A)	0.6853	0.0447	0.5689	0.0505	0.3666	0.0586	0.6728	0.0345
(1,B)	0.6819	0.0790	0.5380	0.0814	0.4608	0.0743	0.4486	0.1209
(1,C)	0.2915	0.0841	0.1993	0.0720	0.1361	0.0586	0.4325	0.0586
(2,A)	0.5781	0.0573	0.4222	0.0553	0.6204	0.0533	0.6499	0.0406
(2,B)	0.6643	0.0258	0.5720	0.0394	0.7147	0.0252	0.4642	0.0369
(3,C)	0.2865	0.0382	0.0999	0.0331	0.1476	0.0203	0.3675	0.0604

the correlation values, compared with the output of the initial alignment stage, is not significant.

Table 7. Average correlation values within sessions per color band of the outputs of the first and second stage of the combined alignment and registration scheme.

Stage	RED	GREEN	BLUE	|B-G|
Initial Alignment	0.7288	0.6377	0.6432	0.7040
Registration (Approach 1)	0.7197	0.6235	0.6329	0.6751
Registration (Approach 2)	0.7412	0.6507	0.6537	0.7412

Table 8. Average correlation values within and between sessions per color band of the outputs of the first and second stage of the combined alignment and registration scheme.

Stage	RED	GREEN	BLUE	|B-G|
Initial alignment	0.5938	0.4935	0.5001	0.5780
Registration (Approach 1)	0.5998	0.4937	0.4915	0.5408
Registration (Approach 2)	0.6114	0.5021	0.5043	0.5741

Regarding the distribution of the noise by comparing pairs of images within a given session, the first session of the registered examples is presented in Appendix E. For the case $(1, A)$, the kind of structure that the M.A.D. Transform [16] detects on the lesion center after the alignment tends to disappear after the registration, however a small structure appears after registration on the top left side of the lesion. For the case $(1, B)$, there is a set of three points that appear on the first absolute M.A.D. component of the first and second capture, that tends to disappear after registration, but at the same time, it tends to appear on the first absolute M.A.D. component of the second and third capture, while it was

not there after the initial alignment. For the case $(1, C)$, structure tends to be noise after registration, but not significantly. Note also that near the borders, the results do not improve much; this is due to the fact that the input to the registration algorithm does not include skin data near the lesion. For the case $(2, A)$ it could be said that the noise tends to be more randomly distributed after registration, the same for the case $(2, B)$. Particularly, for the case $(2, B)$ it has to be mentioned that, by visual assessment, the registration within sessions of images not belonging to the first session look seriously corrupted due to the presence of hair partially covering the lesion. For the case $(3, C)$ it seems that a kind of structure appear after registration, in spite of having increased the correlation within sessions (See Table 14).

Conclusions

The application of the Extreme Value Detection Algorithm during the initial alignment has shown to produce satisfactory results. Results analysis indicates that large variability in the data sets sizes influences the detection of the extreme value.

Two different approaches for pattern registration were proposed. Results indicate that using an average grid (approach 2) produces better registration results than using the first pattern of a given sequence as reference (approach 1) in the registration process. Compared to the outputs of the initial alignment scheme, it has been shown that the second approach used in the second stage of the present scheme improves the correlation between the registered patterns. However, this improvement is not significant. The registration of aligned patterns within and between sessions is clearly not an easy problem.

Acknowledgments

To the SITE Project funded by a grant from the Danish Technical Research Foundation (Project Number *STVF* 56-00-0123) for supporting the present work. To the dermatologists Lone Skov and Bo Bang of the Gentofte Hospital of Denmark and to the anonymous patients, for their collaboration during the image acquisition sessions.

Appendix

A The Initial Alignment Stage Outputs

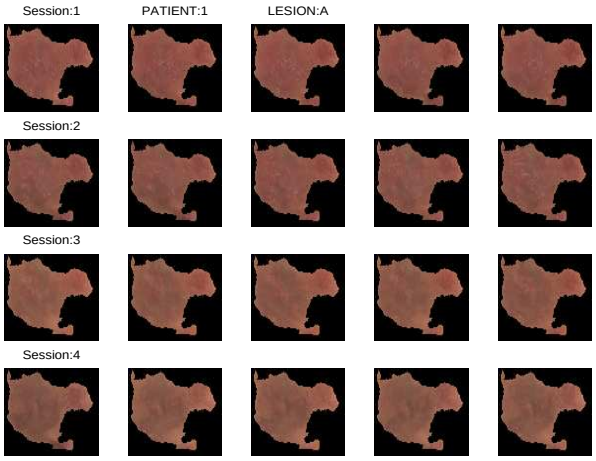

Fig. 4. Initial alignment of lesion patterns for the case (Patient 1, Lesion A).

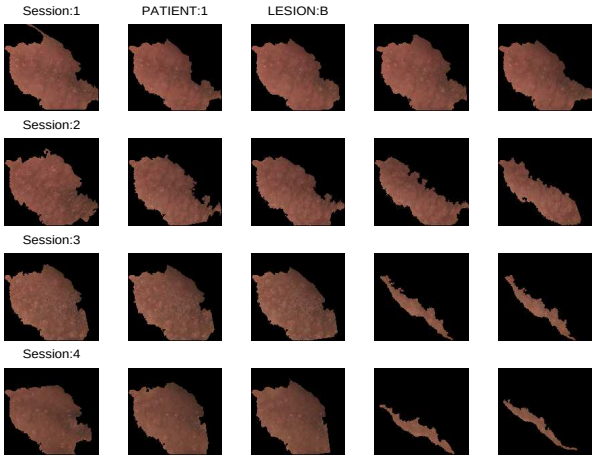

Fig. 5. Initial alignment of lesion patterns for the case (Patient 1, Lesion B).

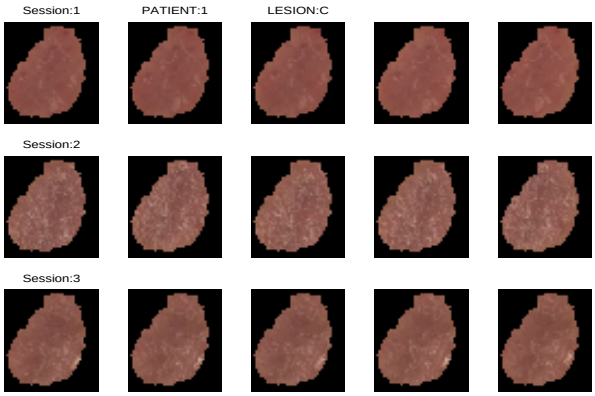

Fig. 6. Initial alignment of lesion patterns for the case (Patient 1, Lesion C).

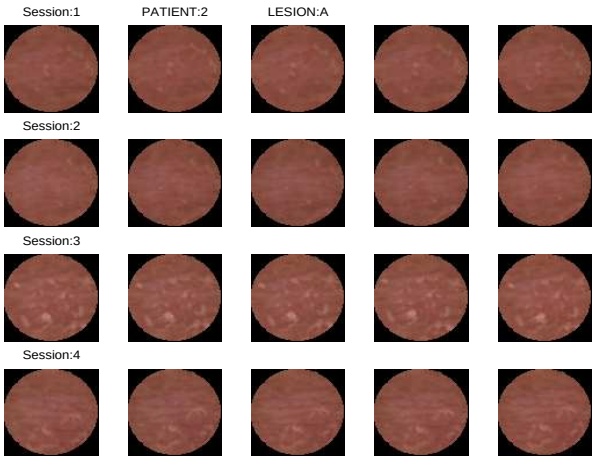

Fig. 7. Initial alignment of lesion patterns for the case (Patient 2, Lesion A).

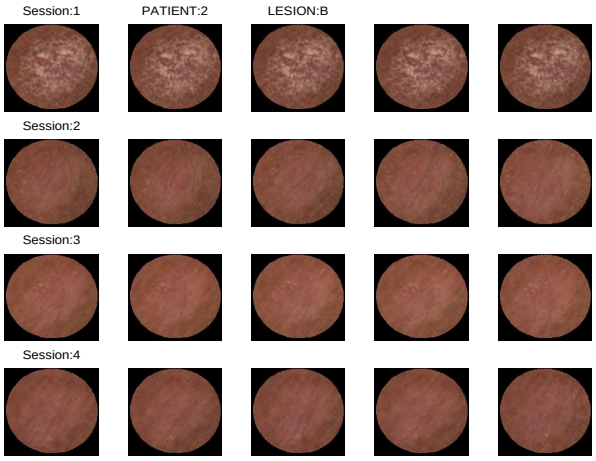

Fig. 8. Initial alignment of lesion patterns for the case (Patient 2, Lesion B).

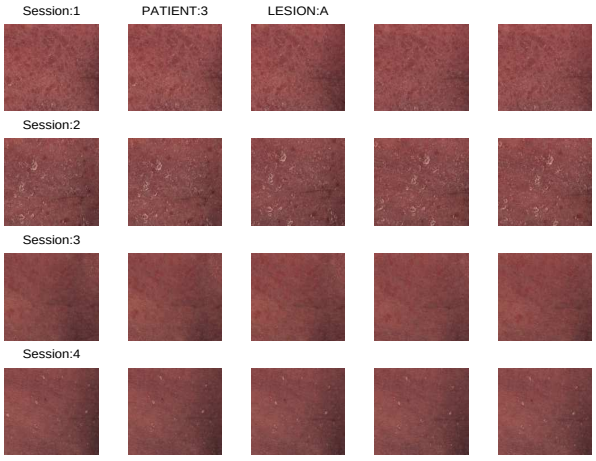

Fig. 9. Initial alignment of lesion patterns for the case (Patient 3, Lesion A).

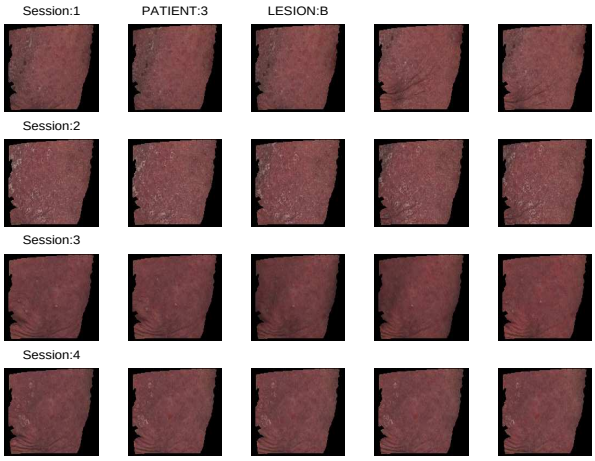

Fig. 10. Initial alignment of lesion patterns for the case (Patient 3, Lesion B).

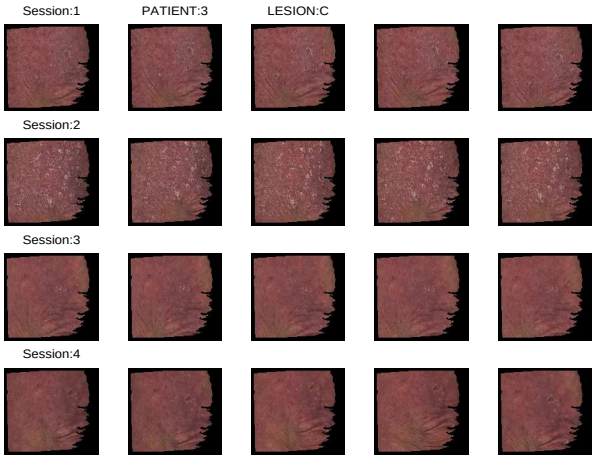

Fig. 11. Initial alignment of lesion patterns for the case (Patient 3, Lesion C).

B Illumination Correction: an example.

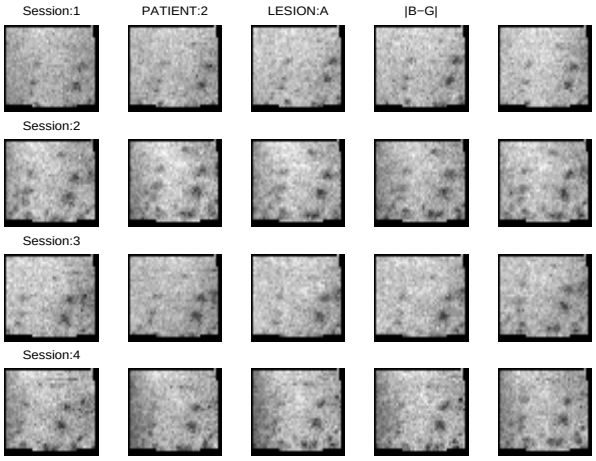

Fig. 12. Initial alignment of lesions for not illumination corrected images of (Patient 2, Lesion A).

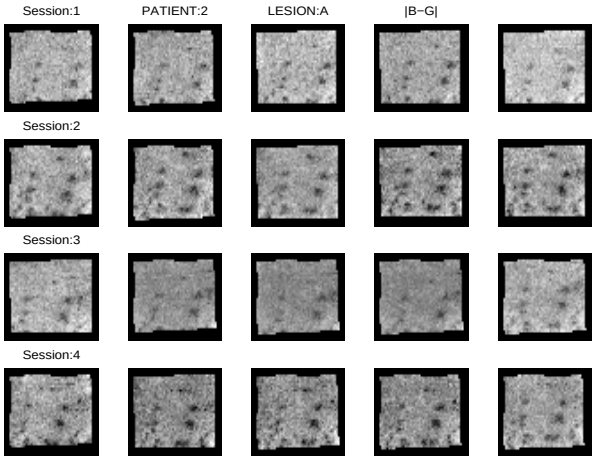

Fig. 13. Initial alignment of lesions for illumination corrected images of (Patient 2, Lesion A).

Table 9. Within and between sessions average correlation and standard deviation of randomly selecting an aligned lesion as reference image for the registration per color band for the case (Patient 2, lesion A).

Before	μ_R	σ_R	μ_G	σ_G	μ_B	σ_B
(a,a)	0.6807	0.1722	0.5122	0.2510	0.5945	0.2114
(a,b)	0.6114	0.0792	0.3953	0.0667	0.4696	0.0544
(a,c)	0.4123	0.0678	0.2339	0.0470	0.3856	0.0442
(a,d)	0.6231	0.0885	0.4071	0.0795	0.5023	0.0630
(b,b)	0.8538	0.0851	0.6993	0.1660	0.7093	0.1566
(b,c)	0.3705	0.0930	0.2052	0.0625	0.3597	0.0548
(b,d)	0.8313	0.0456	0.6579	0.0726	0.6649	0.0533
(c,c)	0.5420	0.2715	0.4259	0.3230	0.5309	0.2694
(c,d)	0.3623	0.0926	0.1963	0.0689	0.3831	0.0557
(d,d)	0.8896	0.0677	0.7763	0.1262	0.7674	0.1284
After	μ_R	σ_R	μ_G	σ_G	μ_B	σ_B
(a,a)	0.5015	0.2620	0.4086	0.3048	0.4218	0.2966
(a,b)	0.2607	0.0819	0.1782	0.0687	0.1491	0.0685
(a,c)	0.2810	0.1361	0.2136	0.1071	0.2031	0.1059
(a,d)	0.2535	0.0763	0.1758	0.0565	0.1562	0.0538
(b,b)	0.4755	0.2707	0.4010	0.3036	0.3429	0.3332
(b,c)	0.2837	0.1233	0.2179	0.0899	0.1712	0.0904
(b,d)	0.3484	0.1030	0.2475	0.0721	0.1756	0.0723
(c,c)	0.5849	0.2579	0.5039	0.2913	0.4614	0.3127
(c,d)	0.3281	0.1006	0.2343	0.0863	0.2001	0.0805
(d,d)	0.5510	0.2403	0.4355	0.2881	0.3798	0.3145

C Registration

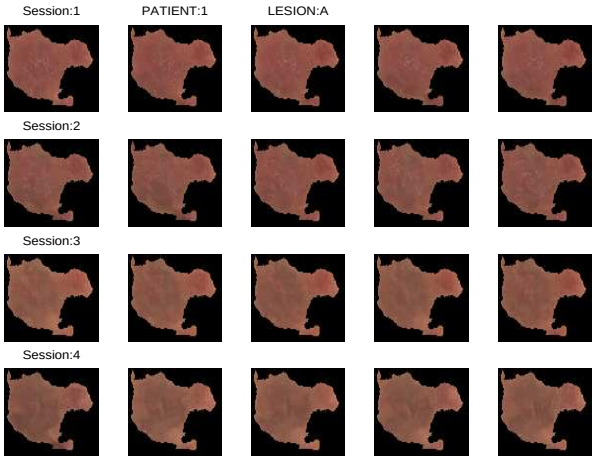

Fig. 14. Registered pattern for the case (Patient 1, Lesion A).

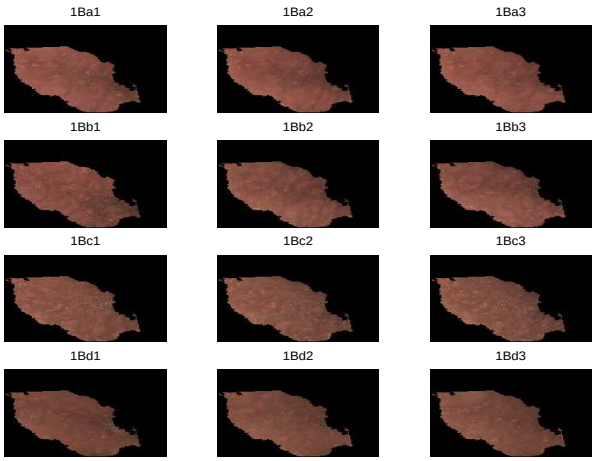

Fig. 15. Registered pattern for the case (Patient 1, Lesion B).

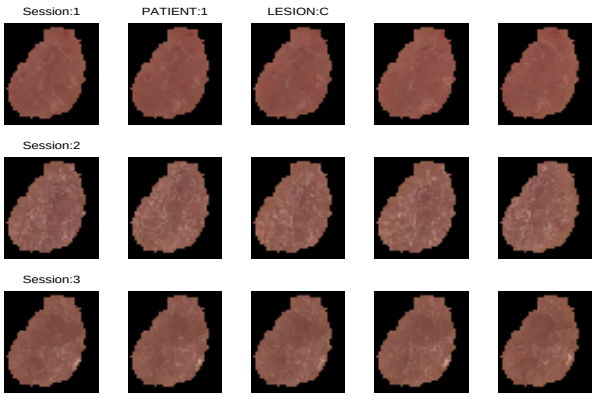

Fig. 16. Registered pattern for the case (Patient 1, Lesion C).

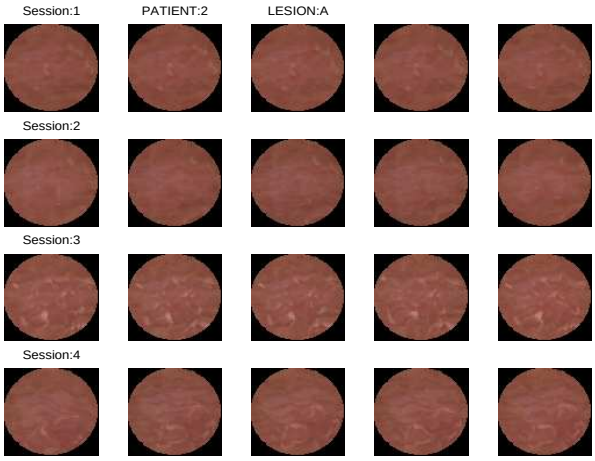

Fig. 17. Registered pattern for the case (Patient 2, Lesion A).

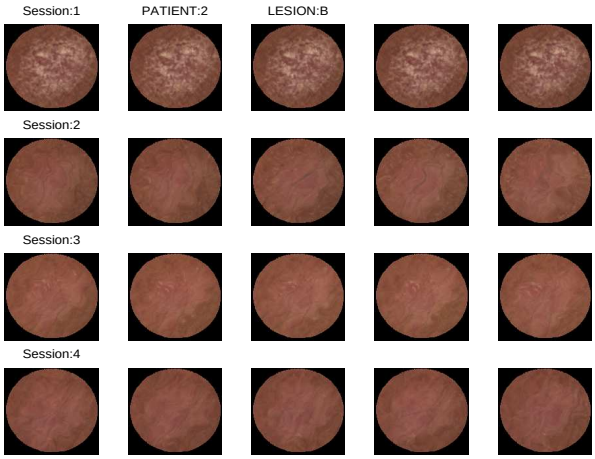

Fig. 18. Registered pattern for the case (Patient 2, Lesion B).

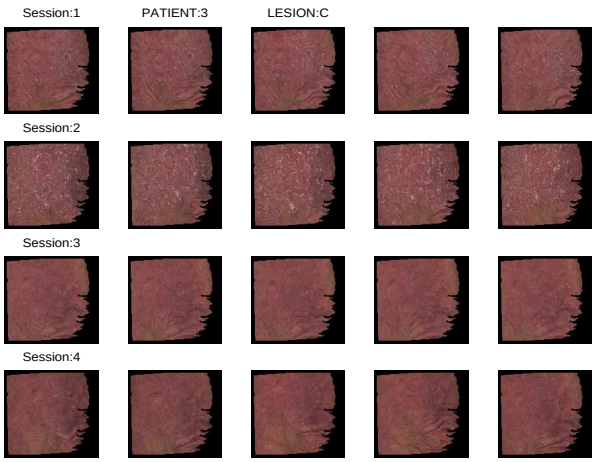

Fig. 19. Registered pattern for the case (Patient 3, Lesion C).

D Result Evaluation

Table 10. Within and between sessions average correlation values of randomly selecting an aligned lesion as reference image for the registration per color band.

Sessions	(1,A)	(1,B)[10]	(1,C)	(2,A)	(2,B)	(3,C)
RED						
(a,a)	0.8305	0.8785	0.5349	0.8612	0.9605	0.5010
(a,b)	0.6642	0.6850	0.1342	0.6632	0.5556	0.2969
(a,c)	0.5949	0.7029	0.2424	0.4274	0.6500	0.1010
(a,d)	0.6055	0.7247		0.3704	0.5728	0.2619
(b,b)	0.8186	0.6231	0.3872	0.8314	0.7772	0.5089
(b,c)	0.6415	0.6096	0.1497	0.4730	0.6796	0.0723
(b,d)	0.5888	0.6129		0.4438	0.6543	0.3045
(c,c)	0.9421	0.8213	0.7540	0.7376	0.8376	0.7408
(c,d)	0.8183	0.6835		0.3676	0.6850	0.1876
(d,d)	0.8973	0.7943		0.7260	0.7847	0.4772
GREEN						
(a,a)	0.7908	0.7915	0.4754	0.7958	0.9609	0.2962
(a,b)	0.5011	0.5695	0.0620	0.4698	0.4892	0.0509
(a,c)	0.5917	0.5108	0.1245	0.2391	0.5475	-0.0291
(a,d)	0.5300	0.5956		0.2302	0.4893	0.0077
(b,b)	0.6839	0.5944	0.3617	0.7490	0.6794	0.3118
(b,c)	0.5128	0.4492	0.0421	0.2439	0.5803	-0.0463
(b,d)	0.4150	0.5050		0.2926	0.5270	0.0962
(c,c)	0.8539	0.6684	0.6921	0.6683	0.7708	0.6197
(c,d)	0.6632	0.4967		0.1903	0.5698	0.0914
(d,d)	0.8133	0.7120		0.6683	0.7022	0.3814
BLUE						
(a,a)	0.6664	0.7584	0.4385	0.8829	0.9692	0.3748
(a,b)	0.3283	0.5201	0.0347	0.7156	0.6348	0.1470
(a,c)	0.3114	0.4066	-0.0106	0.4841	0.6962	0.0296
(a,d)	0.2267	0.4946		0.4555	0.6469	0.0890
(b,b)	0.6092	0.5605	0.3456	0.8528	0.7927	0.3505
(b,c)	0.2874	0.3651	0.0160	0.5204	0.7468	0.0655
(b,d)	0.1183	0.4215		0.5192	0.7149	0.1555
(c,c)	0.7839	0.6090	0.6920	0.7593	0.8653	0.5334
(c,d)	0.5173	0.4063		0.4233	0.7524	0.0944
(d,d)	0.7538	0.6495		0.7626	0.8239	0.3388
|B-G|						
(a,a)	0.8757	0.7140	0.6136	0.8598	0.8423	0.6066
(a,b)	0.7071	0.4475	0.4054	0.7181	0.3133	0.3197
(a,c)	0.7234	0.5563	0.4604	0.6792	0.3059	0.3719
(a,d)	0.6361	0.4538		0.4971	0.3368	0.4287
(b,b)	0.8156	0.5339	0.4991	0.7951	0.6708	0.5283
(b,c)	0.6941	0.4281	0.3274	0.6511	0.5717	0.0902
(b,d)	0.6052	0.3616		0.5642	0.5380	0.2546
(c,c)	0.8232	0.6938	0.6379	0.7986	0.7470	0.7904
(c,d)	0.6730	0.4662		0.5778	0.5499	0.3575
(d,d)	0.7582	0.5891		0.8307	0.6875	0.5860

Table 11. Within and between sessions standard deviation correlation values of randomly selecting an aligned lesion as reference image for the registration per color band.

Sessions	(1,A)	(1,B)	(1,C)	(2,A)	(2,B)	(3,C)
RED						
(a,a)	0.1077	0.1067	0.2948	0.0821	0.0241	0.2542
(a,b)	0.0478	0.1849	0.0766	0.0341	0.0238	0.0665
(a,c)	0.1074	0.0633	0.0385	0.0179	0.0255	0.0317
(a,d)	0.1142	0.0889		0.0253	0.0233	0.0925
(b,b)	0.0994	0.3662	0.4070	0.1050	0.1306	0.2461
(b,c)	0.0750	0.1142	0.0520	0.0240	0.0407	0.0209
(b,d)	0.0801	0.1816		0.0180	0.0265	0.1064
(c,c)	0.0303	0.1396	0.1464	0.1937	0.0919	0.1745
(c,d)	0.0400	0.0676		0.0479	0.0294	0.1081
(d,d)	0.0845	0.1612		0.2042	0.1221	0.2985
GREEN						
(a,a)	0.1151	0.1689	0.3293	0.1345	0.0249	0.3535
(a,b)	0.0337	0.1825	0.0511	0.0526	0.0122	0.0294
(a,c)	0.0697	0.0769	0.0376	0.0259	0.0285	0.0128
(a,d)	0.0929	0.0953		0.0322	0.0261	0.0489
(b,b)	0.1608	0.3508	0.4100	0.1632	0.1882	0.3444
(b,c)	0.0393	0.1180	0.0516	0.0368	0.0398	0.0142
(b,d)	0.0580	0.1752		0.0145	0.0342	0.0650
(c,c)	0.0754	0.2435	0.1838	0.2631	0.1327	0.2504
(c,d)	0.0456	0.0849		0.0522	0.0365	0.0910
(d,d)	0.1246	0.2135		0.2623	0.1651	0.3341
BLUE						
(a,a)	0.1774	0.1889	0.3422	0.0749	0.0193	0.3137
(a,b)	0.0508	0.1681	0.0450	0.0395	0.0157	0.0262
(a,c)	0.0898	0.0775	0.0250	0.0276	0.0223	0.0197
(a,d)	0.1322	0.0824		0.0334	0.0261	0.0412
(b,b)	0.2006	0.3679	0.4304	0.0991	0.1214	0.3250
(b,c)	0.0357	0.1028	0.0406	0.0302	0.0282	0.0121
(b,d)	0.0654	0.1333		0.0182	0.0237	0.0514
(c,c)	0.1112	0.2858	0.1833	0.1911	0.0783	0.3022
(c,d)	0.0497	0.0822		0.0527	0.0229	0.0272
(d,d)	0.1513	0.2553		0.1852	0.0964	0.3476
|B-G|						
(a,a)	0.0641	0.2177	0.2457	0.0767	0.0806	0.2062
(a,b)	0.0279	0.2555	0.1691	0.0467	0.0345	0.0881
(a,c)	0.0196	0.0771	0.0819	0.0217	0.0237	0.0548
(a,d)	0.0296	0.1434		0.0306	0.0185	0.0957
(b,b)	0.0951	0.3882	0.3351	0.1172	0.1811	0.2422
(b,c)	0.0359	0.2225	0.0755	0.0383	0.0398	0.0558
(b,d)	0.0537	0.2142		0.0190	0.0321	0.1128
(c,c)	0.0897	0.2252	0.1933	0.1177	0.1297	0.1154
(c,d)	0.0213	0.1245		0.0475	0.0565	0.1500
(d,d)	0.1313	0.3032		0.0963	0.1625	0.2351

Table 12. Average Correlation Values between pairs of Sessions per Patient, Lesion and Color Band of the outputs of the Registration Approach 1

Sessions	(1,A)	(1,B)	(1,C)	(2,A)	(2,B)	(3,C)
RED						
(a,a)	0.8176	0.8753	0.5962	0.8446	0.9246	0.5469
(a,b)	0.6584	0.6875	0.1892	0.7030	0.5979	0.3246
(a,c)	0.5902	0.6904	0.2724	0.4994	0.6634	0.1512
(a,d)	0.6294	0.7384		0.4391	0.6213	0.2980
(b,b)	0.8030	0.6537	0.3545	0.8044	0.7555	0.5378
(b,c)	0.6222	0.6123	0.1968	0.5354	0.6509	0.1002
(b,d)	0.6062	0.6318		0.4699	0.6366	0.3388
(c,c)	0.9289	0.8168	0.6575	0.6460	0.7953	0.6500
(c,d)	0.8251	0.6864		0.4061	0.6597	0.2088
(d,d)	0.9011	0.8256		0.6855	0.7330	0.4948
GREEN						
(a,a)	0.7641	0.8139	0.5423	0.7589	0.9176	0.3445
(a,b)	0.5118	0.5832	0.1110	0.4900	0.5501	0.0473
(a,c)	0.5650	0.5065	0.1710	0.2717	0.5489	-0.0177
(a,d)	0.5196	0.6106		0.2887	0.5466	0.0189
(b,b)	0.6900	0.6184	0.3260	0.7038	0.6565	0.3322
(b,c)	0.4957	0.4549	0.0921	0.3140	0.5474	-0.0269
(b,d)	0.4229	0.5244		0.3157	0.5333	0.1131
(c,c)	0.8308	0.6739	0.5809	0.5229	0.7155	0.5174
(c,d)	0.6480	0.4956		0.2217	0.5578	0.0941
(d,d)	0.8074	0.7438		0.6134	0.6625	0.3957
BLUE						
(a,a)	0.6284	0.7868	0.5087	0.8732	0.9374	0.4220
(a,b)	0.3351	0.5340	0.0754	0.7275	0.6651	0.1530
(a,c)	0.2945	0.4119	0.0318	0.5228	0.6964	0.0583
(a,d)	0.2450	0.5326		0.4749	0.6768	0.1045
(b,b)	0.5957	0.5862	0.2989	0.8195	0.7614	0.3665
(b,c)	0.2634	0.3680	0.0509	0.5747	0.7027	0.0913
(b,d)	0.1555	0.4477		0.5137	0.6914	0.1690
(c,c)	0.7542	0.6188	0.5790	0.6702	0.8150	0.4418
(c,d)	0.5389	0.4102		0.4376	0.7150	0.1052
(d,d)	0.7531	0.6871		0.7184	0.7793	0.3499
|B-G|						
(a,a)	0.8638	0.7247	0.6234	0.8574	0.7736	0.5611
(a,b)	0.7012	0.4244	0.4127	0.7097	0.2698	0.2867
(a,c)	0.6794	0.4944	0.4469	0.6754	0.2608	0.3194
(a,d)	0.6005	0.3927		0.4274	0.2702	0.3604
(b,b)	0.8005	0.5111	0.4937	0.7636	0.5829	0.5148
(b,c)	0.6335	0.3810	0.3303	0.6355	0.4647	0.0873
(b,d)	0.5608	0.3064		0.4561	0.4486	0.2876
(c,c)	0.7854	0.6755	0.5892	0.7572	0.6817	0.7298
(c,d)	0.6309	0.4144		0.4947	0.4749	0.3389
(d,d)	0.7418	0.5884		0.7919	0.6264	0.5672

Table 13. Standard Deviation of the Correlation Values between pairs of Sessions per Patient, Lesion and Color Band of the outputs of the Registration Approach 1

Sessions	(1,A)	(1,B)	(1,C)	(2,A)	(2,B)	(3,C)
RED						
(a,a)	0.1072	0.0980	0.2416	0.0799	0.0457	0.2467
(a,b)	0.0443	0.1484	0.0890	0.0228	0.0220	0.0656
(a,c)	0.0991	0.0500	0.0540	0.0358	0.0266	0.0288
(a,d)	0.0915	0.0610		0.0565	0.0266	0.0973
(b,b)	0.1074	0.3228	0.3550	0.1019	0.1306	0.2319
(b,c)	0.0744	0.0787	0.0691	0.0344	0.0581	0.0315
(b,d)	0.0723	0.1465		0.0408	0.0389	0.1115
(c,c)	0.0375	0.1379	0.1795	0.1874	0.1078	0.1862
(c,d)	0.0281	0.0612		0.0442	0.0332	0.1048
(d,d)	0.0706	0.1301		0.1670	0.1421	0.2855
GREEN						
(a,a)	0.1262	0.1388	0.2704	0.1251	0.0514	0.3468
(a,b)	0.0285	0.1364	0.0687	0.0404	0.0236	0.0369
(a,c)	0.0650	0.0705	0.0359	0.0440	0.0223	0.0131
(a,d)	0.0716	0.0625		0.0698	0.0265	0.0617
(b,b)	0.1575	0.3197	0.3560	0.1530	0.1847	0.3342
(b,c)	0.0357	0.0931	0.0680	0.0491	0.0402	0.0200
(b,d)	0.0555	0.1439		0.0552	0.0296	0.0735
(c,c)	0.0865	0.2377	0.2195	0.2563	0.1485	0.2499
(c,d)	0.0351	0.0760		0.0509	0.0326	0.0774
(d,d)	0.1206	0.1868		0.2096	0.1754	0.3218
BLUE						
(a,a)	0.1941	0.1549	0.2821	0.0662	0.0384	0.3041
(a,b)	0.0401	0.1142	0.0667	0.0269	0.0168	0.3041
(a,c)	0.0944	0.0674	0.0539	0.0319	0.0168	0.0232
(a,d)	0.1069	0.0562		0.0563	0.0322	0.0490
(b,b)	0.2066	0.3340	0.3763	0.0941	0.1269	0.3170
(b,c)	0.0418	0.0725	0.0442	0.0350	0.0309	0.0178
(b,d)	0.0639	0.1046		0.0526	0.0194	0.0569
(c,c)	0.1251	0.2753	0.2200	0.1803	0.0961	0.2875
(c,d)	0.0380	0.0721		0.0424	0.0273	0.0186
(d,d)	0.1431	0.2253		0.1512	0.1149	0.3356
|B-G|						
(a,a)	0.0699	0.2020	0.2336	0.0721	0.1202	0.2393
(a,b)	0.0247	0.2405	0.1730	0.0355	0.0403	0.0829
(a,c)	0.0221	0.0762	0.0656	0.0187	0.0373	0.0620
(a,d)	0.0317	0.0917		0.0276	0.0380	0.0807
(b,b)	0.1012	0.4065	0.3426	0.1223	0.2168	0.0807
(b,c)	0.0305	0.2088	0.0737	0.0318	0.0396	0.0541
(b,d)	0.0533	0.1721		0.0336	0.0596	0.1229
(c,c)	0.1094	0.2375	0.2095	0.1265	0.1633	0.1229
(c,d)	0.0262	0.0889		0.0609	0.0574	0.1412
(d,d)	0.1435	0.2987		0.1131	0.1903	0.2487

Table 14. Average Correlation Values between pairs of Sessions per Patient, Lesion and Color Band of the outputs of the Registration Approach 2

Sessions	(1,A)	(1,B)	(1,C)	(2,A)	(2,B)	(3,C)
RED						
(a,a)	0.8250	0.8922	0.6495	0.9003	0.9636	0.5667
(a,b)	0.6719	0.6866	0.1831	0.7215	0.5699	0.3209
(a,c)	0.5981	0.6911	0.2977	0.5147	0.6606	0.1492
(a,d)	0.5972	0.7488		0.4643	0.6060	0.3074
(b,b)	0.8092	0.6412	0.3612	0.8457	0.7605	0.5333
(b,c)	0.6299	0.5996	0.1686	0.5429	0.6568	0.0907
(b,d)	0.5760	0.6348		0.4982	0.6300	0.3319
(c,c)	0.9290	0.8543	0.7393	0.7548	0.8154	0.6925
(c,d)	0.8145	0.6987		0.4422	0.6717	0.2241
(d,d)	0.8778	0.8276		0.7182	0.7676	0.5144
GREEN						
(a,a)	0.7785	0.8244	0.5844	0.8599	0.9650	0.3761
(a,b)	0.5124	0.5774	0.1089	0.5268	0.5209	0.0600
(a,c)	0.5947	0.5096	0.1745	0.3343	0.5596	0.0004
(a,d)	0.5198	0.6188		0.3088	0.5361	0.0391
(b,b)	0.6795	0.6061	0.3288	0.7683	0.6610	0.3309
(b,c)	0.5028	0.4351	0.0595	0.3299	0.5444	-0.0326
(b,d)	0.4031	0.5178		0.3501	0.5068	0.1139
(c,c)	0.8271	0.7162	0.6751	0.6879	0.7275	0.5767
(c,d)	0.6526	0.5130		0.2730	0.5586	0.1269
(d,d)	0.7918	0.7331		0.6548	0.6887	0.4191
BLUE						
(a,a)	0.6528	0.7969	0.5471	0.9189	0.9726	0.4414
(a,b)	0.3419	0.5264	0.0621	0.7517	0.6416	0.1600
(a,c)	0.3245	0.4076	0.0343	0.5558	0.6988	0.0524
(a,d)	0.2304	0.5305		0.5258	0.6704	0.1160
(b,b)	0.5966	0.5750	0.3050	0.8648	0.7701	0.3651
(b,c)	0.2723	0.3508	0.0164	0.5802	0.7090	0.0757
(b,d)	0.1142	0.4407		0.5583	0.6890	0.1680
(c,c)	0.7514	0.6714	0.6658	0.7739	0.8348	0.4935
(c,d)	0.5358	0.4292		0.4855	0.7314	0.1178
(d,d)	0.7331	0.6783		0.7582	0.8063	0.3631
|B-G|						
(a,a)	0.8701	0.7391	0.6490	0.8715	0.8455	0.6351
(a,b)	0.6960	0.4479	0.4141	0.7355	0.3003	0.3535
(a,c)	0.7084	0.5506	0.4755	0.6811	0.3018	0.3826
(a,d)	0.6240	0.4588		0.5097	0.3445	0.4076
(b,b)	0.8021	0.5310	0.4797	0.7971	0.6276	0.5532
(b,c)	0.6640	0.4185	0.3429	0.6593	0.5243	0.1153
(b,d)	0.5886	0.3559		0.5416	0.4965	0.3061
(c,c)	0.7955	0.7039	0.6391	0.7956	0.7214	0.7548
(c,d)	0.6291	0.4492		0.5739	0.5254	0.3608
(d,d)	0.7384	0.5778		0.8129	0.6750	0.5915

Table 15. Standard Deviation of the Correlation Values between pairs of Sessions per Patient, Lesion and Color Band of the outputs of the Registration Approach 2

Sessions	(1,A)	(1,B)	(1,C)	(2,A)	(2,B)	(3,C)
RED						
(a,a)	0.1085	0.0879	0.2196	0.0525	0.0207	0.2369
(a,b)	0.0450	0.1529	0.0729	0.0199	0.0149	0.0742
(a,c)	0.1049	0.0549	0.0429	0.0125	0.0242	0.0365
(a,d)	0.1201	0.0668		0.0276	0.0280	0.0938
(b,b)	0.1046	0.3420	0.3705	0.0850	0.1410	0.2349
(b,c)	0.0817	0.0915	0.0539	0.0182	0.0465	0.0264
(b,d)	0.0946	0.1492		0.0266	0.0466	0.1017
(c,c)	0.0371	0.1114	0.1419	0.1375	0.0995	0.1641
(c,d)	0.0435	0.0662		0.0254	0.0299	0.1052
(d,d)	0.0986	0.1320		0.1804	0.1293	0.2712
GREEN						
(a,a)	0.1204	0.1352	0.2655	0.0782	0.0202	0.3337
(a,b)	0.0338	0.1489	0.0617	0.0437	0.0128	0.0383
(a,c)	0.0706	0.0674	0.0260	0.0227	0.0284	0.0138
(a,d)	0.0954	0.0808		0.0386	0.0329	0.0637
(b,b)	0.1629	0.3404	0.3722	0.1288	0.1871	0.3354
(b,c)	0.0348	0.0971	0.0659	0.0288	0.0439	0.0170
(b,d)	0.0682	0.1429		0.0343	0.0463	0.0670
(c,c)	0.0887	0.2079	0.1767	0.1797	0.1457	0.2215
(c,d)	0.0548	0.0784		0.0361	0.0288	0.0797
(d,d)	0.1390	0.1966		0.2288	0.1672	0.3089
BLUE						
(a,a)	0.1828	0.1516	0.2785	0.0429	0.0156	0.2986
(a,b)	0.0517	0.1311	0.0660	0.0279	0.0212	0.0287
(a,c)	0.0958	0.0651	0.0332	0.0156	0.0214	0.0245
(a,d)	0.1356	0.0753		0.0319	0.0285	0.0471
(b,b)	0.2050	0.3543	0.3936	0.0757	0.1284	0.3186
(b,c)	0.0351	0.0797	0.0473	0.0251	0.0387	0.0168
(b,d)	0.0828	0.1154		0.0353	0.0423	0.0485
(c,c)	0.1267	0.2383	0.1821	0.1324	0.0882	0.2629
(c,d)	0.0554	0.0790		0.0282	0.0228	0.0280
(d,d)	0.1656	0.2361		0.1543	0.1040	0.3298
|B-G|						
(a,a)	0.0668	0.1926	0.2155	0.0658	0.0785	0.1927
(a,b)	0.0334	0.2376	0.1468	0.0412	0.0717	0.0917
(a,c)	0.0190	0.0684	0.0695	0.0242	0.0411	0.0514
(a,d)	0.0314	0.1222		0.0238	0.0224	0.0783
(b,b)	0.1031	0.3907	0.3391	0.1076	0.1990	0.2360
(b,c)	0.0308	0.2195	0.0693	0.0299	0.0388	0.0703
(b,d)	0.0535	0.2001		0.0128	0.0476	0.1310
(c,c)	0.1037	0.2167	0.1870	0.1094	0.1427	0.1275
(c,d)	0.0348	0.1167		0.0452	0.0498	0.1400
(d,d)	0.1423	0.3082		0.1083	0.1653	0.2322

E First M.A.D. Component of pairs of registered patterns of the same session

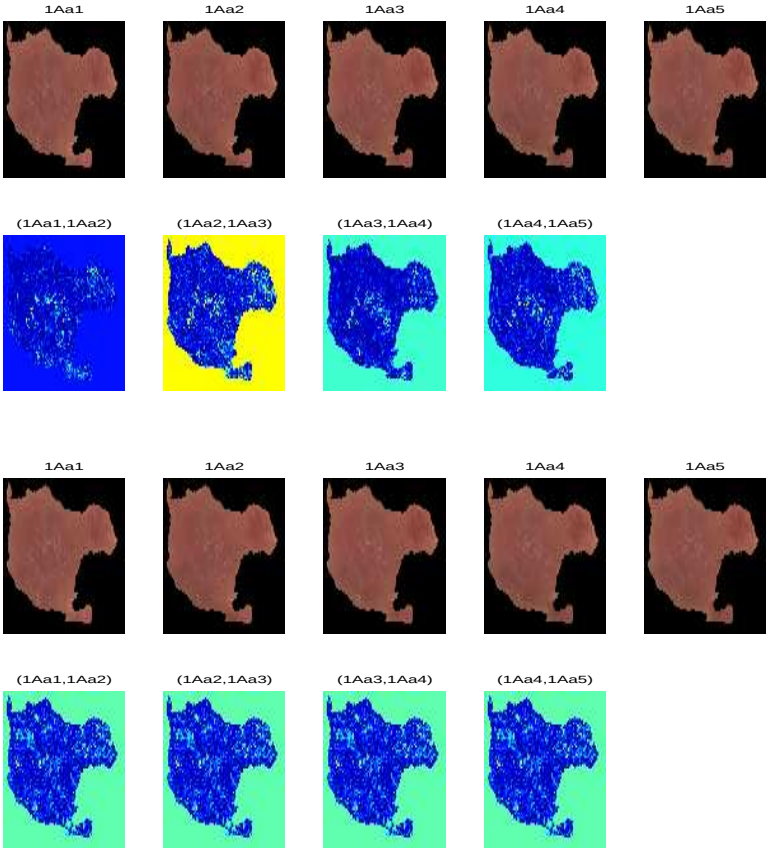

Fig. 20. Images of the first session of the case $(1, A)$ before (top) and after (bottom) registration, and respective first M.A.D. components

References

1. M. Amadasum and R. King. Some texture measures for image segmentation. *Canadian Journal of Electrical and Computer Engineering*, 15(1):18–21, 1990.
2. M. Bolduc and M. Levine. A real-time foveated sensor with overlapping receptive fields. *Real-Time Imaging*, (3):195–212, 1997.

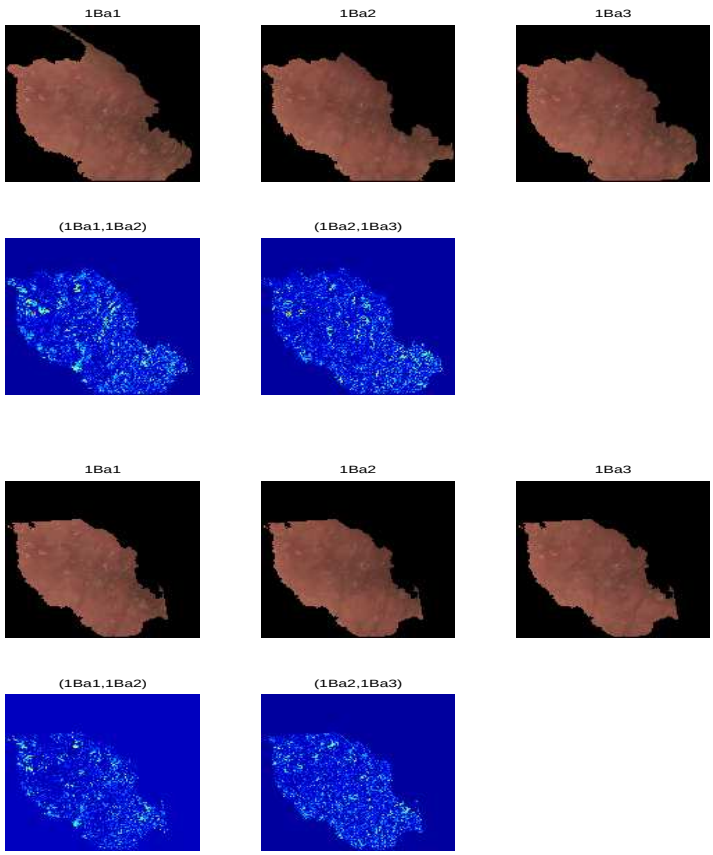

Fig. 21. Images of the first session of the case $(1, C)$ before (top) and after (bottom) registration, and respective first M.A.D. components

3. I. Dryden and K. Mardia. *Statistical Shape Analysis*, volume 1. John Wiley and Sons Ltd., West Sussex, England, 1998.
4. R. Duda and P. Hart. *Pattern Classification and Scene Analysis.* ISBN 0-471-22361-1. John Wiley & Sons, California, 1973.
5. A. Gordon. *Classification. Monographs on Applied Probability and Statistics.* ISBN 0-412-22850-5. Chapman and Hall and Methuen, Inc., London, 1981.
6. R. Haralick. Statistical and structural approaches to texture. *Proceedings of the IEEE*, 67(5):786–804, May 1979.
7. D. He and L. Wang. Texture features based on texture spectrum. *Pattern Recognition*, 24(5):391–399, 1991.
8. K. Hilger. *Exploratory Analysis of Multivariate Data.* Ph.d. thesis, Informatics and Mathematical Modelling. Technical University of Denmark., Kgs. Lyngby, November 2001.

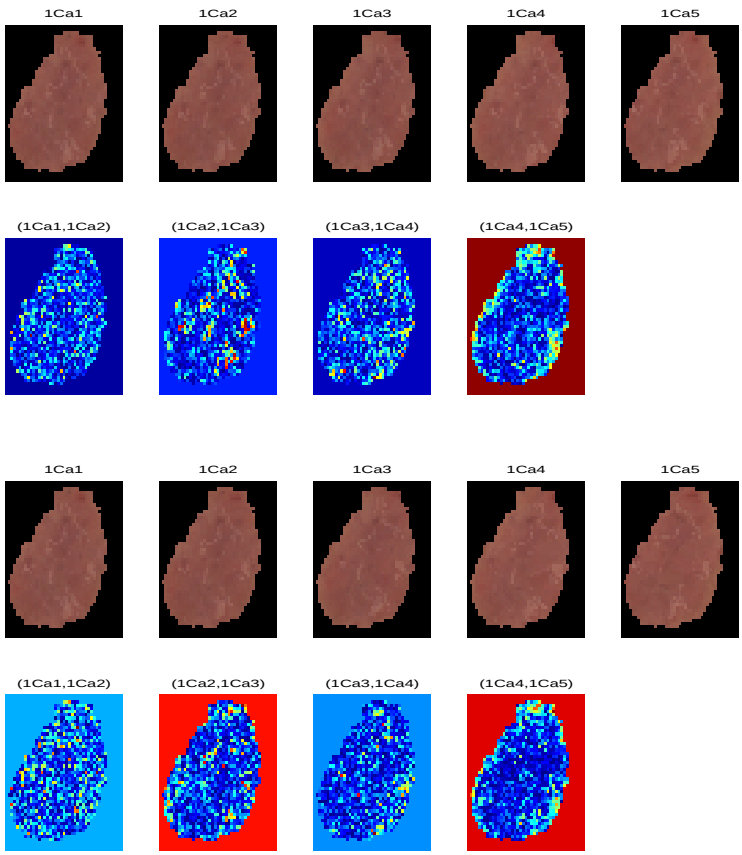

Fig. 22. Images of the first session of the case $(1, C)$ before (top) and after (bottom) registration, and respective first M.A.D. components

9. J. Lira. *Introducción al Tratamiento Digital de Imágenes.* Instituto Politécnico Nacional, Universidad Nacional Autónoma de México, Fondo de Cultura Económica., México D.F., 1 edition, September 2002.
10. J. Lira and G. Maletti. A supervised classifier for multispectral and textured images based on an automated region growing algorithm. *European Space Agency Publications*, SP-434:153–158, 1998.
11. G. Maletti and B. Ersbøll. A hierarchical classification scheme of psoriasis images. Technical Report 6, Department of Informatics and Mathematical Modelling. Technical University of Denmark., Kgs. Lyngby. Denmark., March 2003.
12. G. Maletti and B. Ersbøll. Illumination correction in psoriasis lesions images. Technical Report 7, Department of Informatics and Mathematical Modelling. Technical University of Denmark., Kgs. Lyngby. Denmark., March 2003.
13. G. Maletti and B. Ersbøll. Principal component analysis of psoriasis lesions images. Technical Report 5, Department of Informatics and Mathematical Modelling.

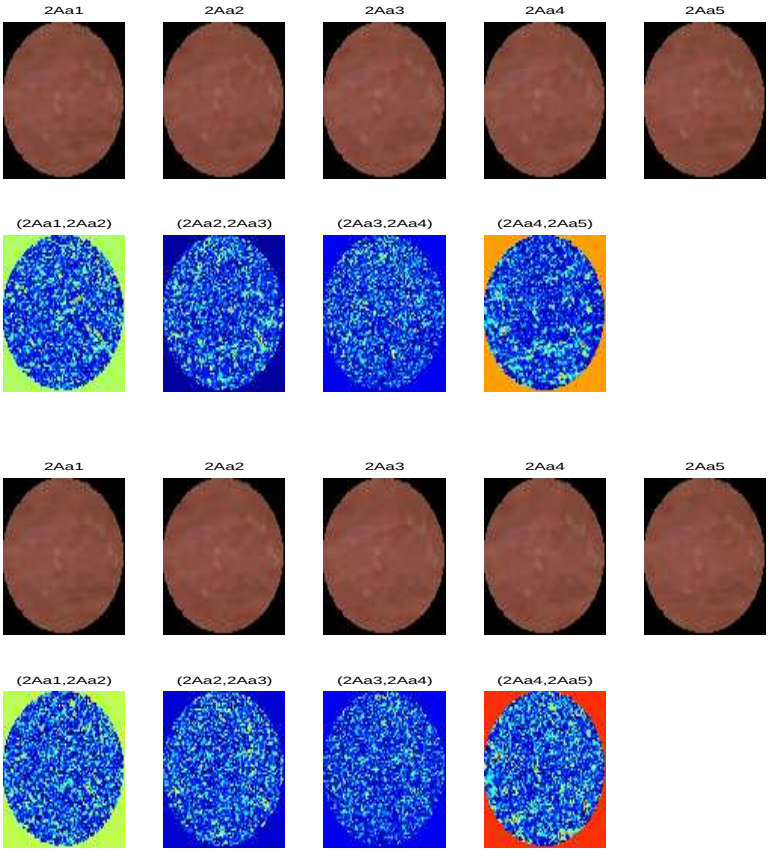

Fig. 23. Images of the first session of the case $(2, A)$ before (top) and after (bottom) registration, and respective first M.A.D. components

Technical University of Denmark., Kgs. Lyngby. Denmark., March 2003.

14. G. Maletti and B. Ersbøll. Texture alteration detection in bitemporal images of lesions with psoriasis. Technical Report 8, Department of Informatics and Mathematical Modelling. Technical University of Denmark., Kgs. Lyngby. Denmark., March 2003.
15. K. Mardia, J. Kent, and J. Bibby. *Multivariate Analysis*. Academic Press, Inc., San Diego, CA92101, 10 edition, 1979.
16. A. Nielsen, K. Conradsen, and J. Simpson. Multivariate alteration detection (m.a.d.) and m.a.f. postprocessing in multispectral, bitemporal image data: New approaches to change detection studies. *Remote Sens. Environ.*, 64:1–19, 1998.
17. M. Sonka, V. Hlavac, and R. Boyle. *Image Processing, Analysis and Machine Vision*. Brooks Cole Publishing Company, Pacific Grove, CA 93950, USA., 2nd edition, 1999.

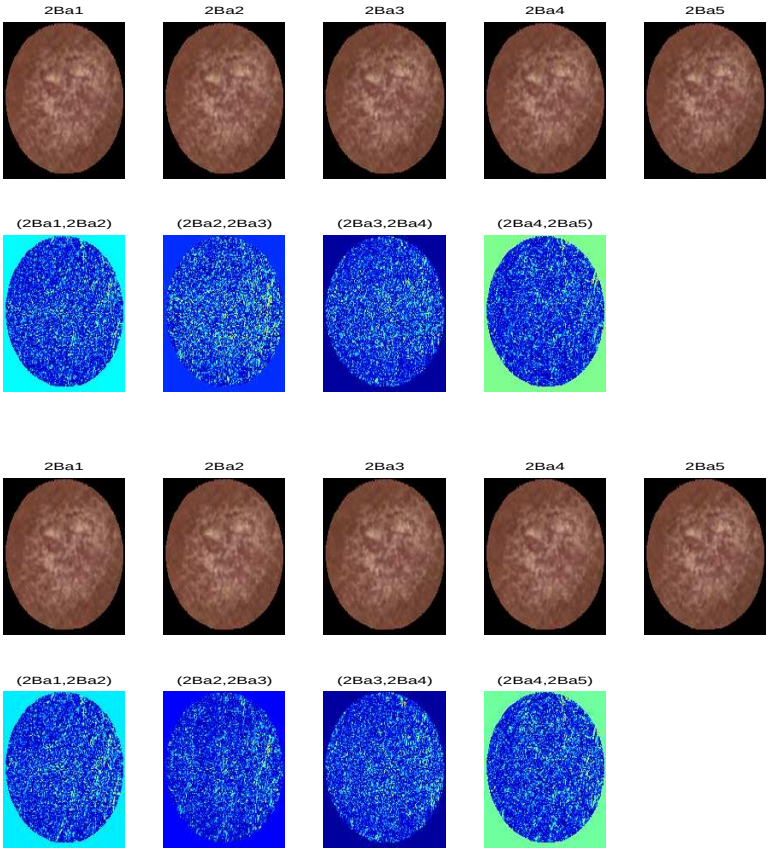

Fig. 24. Images of the first session of the case $(2, B)$ before (top) and after (bottom) registration, and respective first M.A.D. components

18. M. Stegmann. Active appearance models: Theory, extensions and cases. Master's thesis, Informatics and Mathematical Modelling, Technical University of Denmark, DTU, 2000.
19. L. Wang. Vector choice in the texture spectrum approach. *International Journal of Remote Sensing*, 15(18):3823–3829, 1994.
20. L. Wang and D. He. Texture classification using texture spectrum. *Pattern Recognition*, 23(8):905–910, 1990.
21. R. Wilson and T. Martinez. Improved heterogeneous distance function. *Journal of Artificial Intelligence Research*, (6):1–34, 1997.
22. S. Wilson. On the retino-cortical mapping. *International Journal of Man-Machine Studies*, 18(4):361–389, 1983.

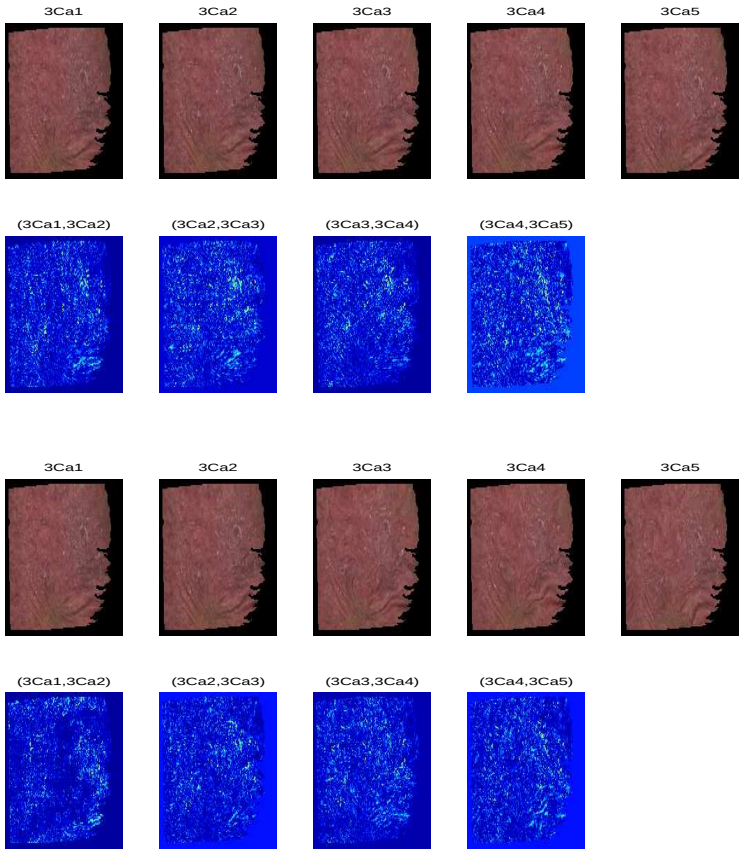

Fig. 25. Images of the first session of the case $(3, C)$ before (top) and after (bottom) registration, and respective first M.A.D. components